Contact-dependent promotion of cell migration by the OL-protocadherin–Nap1 interaction

Shinsuke Nakao,[1,2] Anna Platek,[2] Shinji Hirano,[2] and Masatoshi Takeichi[2]

[1]Graduate School of Biostudies, Kyoto University, Sakyo-ku, Kyoto 606-8501, Japan
[2]RIKEN Center for Developmental Biology, Chuo-ku, Kobe 650-0047, Japan

OL-protocadherin (OL-pc) is a transmembrane protein belonging to the cadherin superfamily, which has been shown to accumulate at cell–cell contacts via its homophilic interaction, but its molecular roles remain elusive. In this study, we show that OL-pc bound Nck-associated protein 1 (Nap1), a protein that regulates WAVE-mediated actin assembly. In astrocytoma U251 cells not expressing OL-pc, Nap1 was localized only along the lamellipodia. However, exogenous expression of OL-pc in these cells recruited Nap1 as well as WAVE1 to cell–cell contact sites. Although OL-pc expression had no effect on the motility of solitary U251 cells, it accelerated their movement when they were in contact with one another, causing concomitant reorganization of F-actin and N-cadherin at cell junctions. OL-pc mutants lacking the Nap1-binding site exhibited no such effect. N-cadherin knockdown mimicked OL-pc expression in enhancing cell movement. These results suggest that OL-pc remodels the motility and adhesion machinery at cell junctions by recruiting the Nap1–WAVE1 complex to these sites and, in turn, promotes the migration of cells.

Introduction

Cell migration plays pivotal roles in animal morphogenesis and is known to be controlled by several molecular mechanisms. Major players in such control mechanisms include actin and microtubule cytoskeletons and their biochemical modulators (Pollard and Borisy, 2003; Watanabe et al., 2005; Takenawa and Suetsugu, 2007). Through the interplay among these components, cells develop various types of motile structures, such as filopodia and lamellipodia, which are essential for the directional migration of cells (Ridley et al., 2003). At the cellular level, cell–cell contacts play a role in the regulation of cell motility, which is well known as contact inhibition of cell movement. When migrating cells meet each other, the membrane ruffling of cell peripheries stops at the contact sites, resulting in suppression of further movement of the cells (Abercrombie and Ambrose, 1958; Abercrombie, 1967). However, the molecular mechanisms underlying the contact-dependent regulation of cell movement are still not fully understood, although the involvement of several molecules such as cadherin and integrin (Chen and Obrink, 1991; Bracke et al., 1997; Huttenlocher et al., 1998), Necl-5 and nectin-3 (Fujito et al., 2005), and Eph-ephrin (Smith et al., 1997; Marston et al., 2003) has been suggested.

OL-protocadherin (OL-pc; protocadherin-10) is a member of the cadherin superfamily (Hirano et al., 2003). As seen with the classical cadherins, OL-pc shows the homophilic binding nature, which can induce cell aggregation when expressed in cadherin-deficient cells (Hirano et al., 1999). However, the ability of OL-pc to promote cell aggregation is much weaker compared with that of classical cadherins (Hirano et al., 1999), raising the possibility that OL-pc might have other functions than the simple physical linking of cells. Our recent analysis of OL-pc knockout mice demonstrated that in the OL-pc–deficient brain, striatal neurons could not normally extend their axons (Uemura et al., 2007). In the wild-type brain, striatal axons project the substantial nigra, whereas in the OL-pc mutants, this projection was missing, as the mutant axons were stalled by clumping together during the early periods of extension. The axon elongation defects were also observed when striatal tissues had been isolated and cultured in vitro. OL-pc was localized along axons, being most highly

Correspondence to Shinji Hirano: s-hirano@cdb.riken.jp; or Masatoshi Takeichi: takeichi@cdb.riken.jp

Abbreviations used in this paper: Abi, Abl interactor; Arp, actin-related protein; CYFIP, cytoplasmic interacting FMR1 protein; Nap1, Nck-associated protein 1; NBS, Nap1-binding site; OL-pc, OL-protocadherin.

The online version of this article contains supplemental material.

The Rockefeller University Press $30.00
J. Cell Biol. Vol. 182 No. 2 395–410
www.jcb.org/cgi/doi/10.1083/jcb.200802069

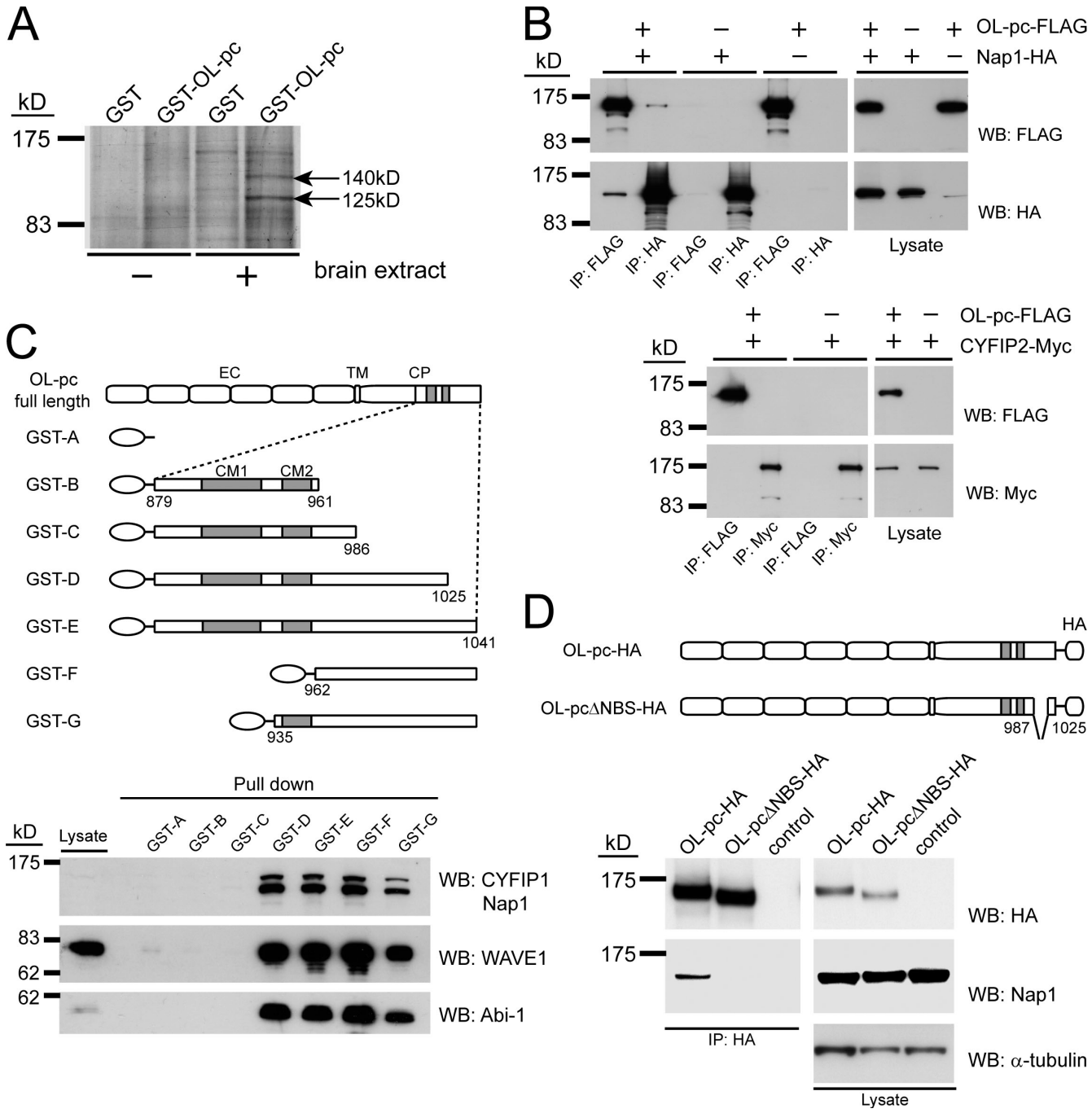

Figure 1. **OL-pc associates with the Nap1–WAVE complex.** (A) A lysate of newborn mouse brain was incubated with GST or the GST-fused cytoplasmic domain OL-pc (GST–OL-pc). Proteins pulled down with these recombinants were separated by SDS-PAGE and detected by silver staining. Bands of 140 kD and 125 kD were identified as CYFIP2 and Nap1, respectively. (B) Coprecipitation of OL-pc with Nap1 but not with CYFIP2. COS7 cells were transiently transfected with plasmids for FLAG-tagged OL-pc, HA-tagged Nap1, or both (top) or with Myc-tagged CYFIP2 or it and FLAG-tagged OL-pc (bottom), and their lysates were processed for immunoprecipitation (IP) with antibodies against the tags. Vain vectors were used for negative controls (−). Precipitated products separated by SDS-PAGE were detected by Western blotting (WB) with the indicated antibodies. (C) GST fusion proteins containing the OL-pc cytoplasmic domain with various deletions (top) and their interaction with components of the Nap1–WAVE complex (bottom). EC, extracellular; TM, transmembrane; CP, cytoplasmic. CM1 and CM2 represent the portions conserved in this protein family. In the bottom panel, these fusion proteins were incubated with a 1-d-old mouse brain lysate, and the proteins pulled down were analyzed. In the top blot, CYFIP1 (top) and Nap1 (bottom) were detected simultaneously by mixing the antibodies against them. We could not test for CYFIP2 in this assay because of the unavailability of antibodies against this molecule. (D) Schematic diagrams for HA-tagged OL-pc without and with the Nap1-binding region (top) and their interaction with Nap1 (bottom). U251 cells were stably transfected with OL-pc-HA, OL-pcΔNBS-HA, or control vectors, and immunoprecipitates obtained with anti-HA tag antibodies from their lysates were analyzed by Western blotting. α-Tubulin was used for a loading control.

concentrated in their growth cones. These observations suggested that OL-pc played a role in sustaining the normal migration of striatal axons.

To investigate the molecular role of OL-pc, we screened for proteins that interact with this protocadherin and identified Nck-associated protein 1 (Nap1) as an OL-pc partner. Nap1,

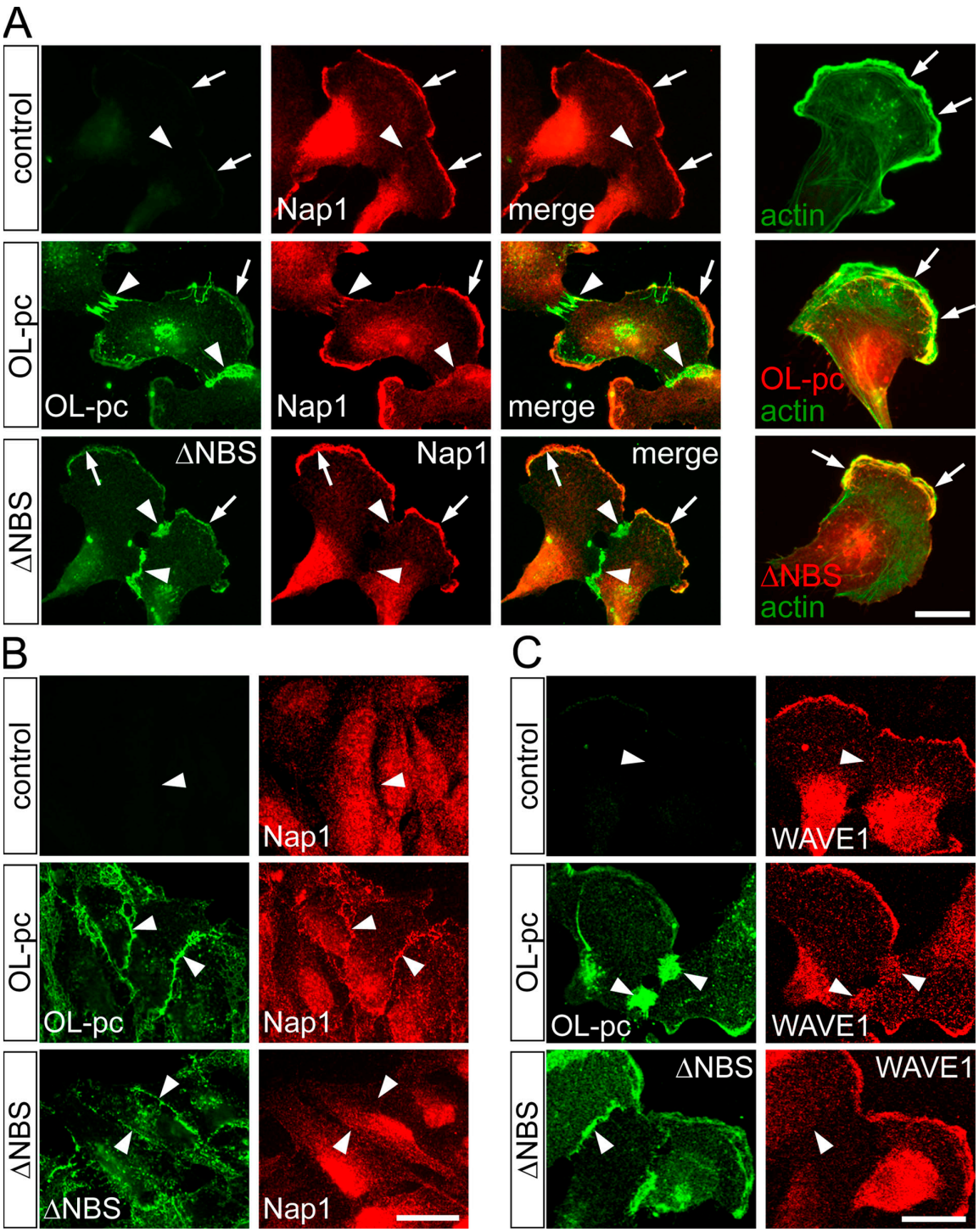

Figure 2. **OL-pc recruits Nap1 and WAVE1 to cell–cell contacts.** (A, left) Control (vain vector transfected) U251 cells and those stably expressing OL-pc-HA or OL-pcΔNBS-HA were cultured in a low density and double immunostained for Nap1 and HA tag. Arrows point to Nap1-positive lamellipodia, and arrowheads here as well as in B and C indicate cell–cell contact sites. Note that Nap1 is localized at cell–cell contacts in the transfectants of OL-pc but not in those of OL-pcΔNBS. (right) Double staining for F-actin and HA. Both OL-pc and OL-pcΔNBS colocalize with F-actin in the lamellipodia. (B) Cells in confluent cultures were double immunostained for Nap1 and HA after extraction with 0.5% Triton X-100. (C) WAVE1-GFP was transiently introduced into cells followed by double immunostaining for OL-pc and GFP. Note the accumulation of WAVE1 at OL-pc–positive but not OL-pcΔNBS–positive cell–cell contact sites. Images were taken with a CCD camera for A and B and with a confocal microscope for C. Bars, 20 μm.

which is widely conserved among various organisms, organizes a molecular complex comprising itself, Sra-1/PIR121/cytoplasmic interacting FMR1 protein (CYFIP), Abl interactor (Abi), and HSPC300 as well as Scar/WAVE (Ibarra et al., 2005). The activity of Scar/WAVE is regulated by the formation of this complex, and through this machinery, upstream Rac1 signals are relayed to the actin-related protein (Arp) 2/3 complex to induce lamellipodia formation (Stradal and Scita, 2006). Although depletion

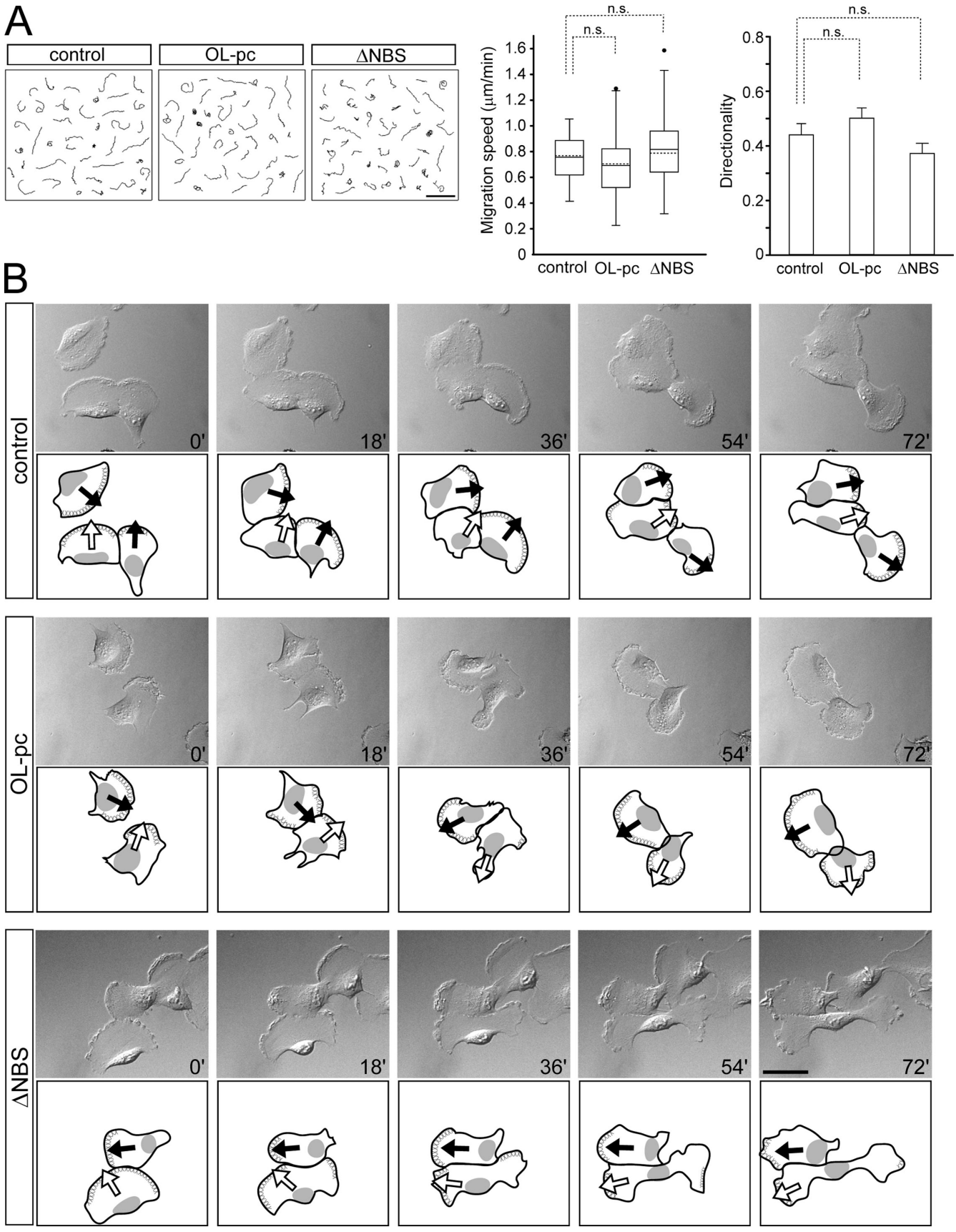

Figure 3. **OL-pc has no effect on single-cell migration but does affect cell-contacting behavior.** (A) Control U251 cells and those stably expressing OL-pc-HA or OL-pcΔNBS-HA were cultured at a low density, and their phase-contrast time-lapse images were taken for 4 h at 3-min intervals. (left) Tracks of individual cells were collected. Only those not dividing and not in contact with others were sampled. (middle) Statistical analysis of the instantaneous velocities of

of Nap1 abrogates lamellipodia formation (Steffen et al., 2004), it allows filopodia formation (Steffen et al., 2006), indicating that Nap1 regulates only restricted portions of the cellular motility machinery. Analysis of the *Dictyostelium discoideum* homologue of the Nap1 gene (*napA*) suggested that Nap1 regulates not only Scar/WAVE but also other cellular activities (Ibarra et al., 2006). In vivo, Nap1 is important for various morphogenetic events, such as neural tube closure and migration of endoderm and mesoderm (Rakeman and Anderson, 2006). In the nervous system, Nap1 is required for neurite extension (Yokota et al., 2007), and its *Drosophila melanogaster* homologue, KETTE, regulates axon pathfinding (Hummel et al., 2000).

The aforementioned functions of Nap1 suggested its potential involvement in OL-pc–dependent cell or axon migration. To test this idea, we constructed a model cell system by using U251 cells, a human astrocytoma line (Vaheri et al., 1976), which exhibited high locomotive nature. We transfected these cells with OL-pc cDNA and compared them with the parent U251 cells to assess the role of the OL-pc–Nap1 complex in cell behavior. In control U251 cells, Nap1 was localized along the lamellipodia of moving cells but not at their cell–cell contact sites that were quiescent in terms of membrane ruffling. However, OL-pc expression in these cells caused a recruitment of not only Nap1 but also WAVE1 to the cell–cell contact sites. The OL-pc–expressing cells exhibited accelerated migration only when they were in contact with others, concomitant with altering the assembly of F-actin and N-cadherin at cell–cell contacts. OL-pc mutants, which lacked the Nap1-binding site (NBS), had no such effects on cell behavior. Furthermore, depletion of Nap1 and WAVE1 abrogated, at least in part, the aforementioned effects of OL-pc on cell motility, and N-cadherin knockdown mimicked the effects of OL-pc expression. Based on these observations, we propose that signals generated by the OL-pc–Nap1 complex at cell–cell contact sites modulate junctional actin organization, perturbing cadherin-based adherens junctions and thereby enhancing cell migration.

Results

Binding of OL-pc with the Nap1–CYFIP complex

To search for proteins that interact with the cytoplasmic domain of OL-pc, we constructed a fusion protein consisting of GST and part of the OL-pc cytoplasmic domain (aa 879–1,041) and analyzed the molecules in lysates of newborn mouse brain that coprecipitated with this construct. We detected two proteins of 125 kD and 140 kD that specifically bound the fusion protein (Fig. 1 A) and identified them as Nap1 and CYFIP2, respectively, by mass spectrometry. To further analyze how these proteins were associated with OL-pc, we cotransfected COS-7 cells with FLAG-tagged OL-pc and HA-tagged Nap1 or myc-tagged CYFIP2 and immunoprecipitated OL-pc from these cells. The results showed that Nap1 coprecipitated with OL-pc, whereas CYFIP2 did not (Fig. 1 B). Because these two proteins are known to form a complex (Ibarra et al., 2005), CYFIP2 likely coprecipitated with OL-pc via the binding to Nap1 in the original pull-down assays. We further tested whether other components of the Nap1–CYFIP complex could be coprecipitated with OL-pc. Immunoblot analysis of the materials pulled down with GST–OL-pc from brain lysates detected WAVE1 and Abi-1 (Fig. 1 C, bottom), suggesting that the OL-pc–associated Nap1 formed its well-known complex with the other partners (Ibarra et al., 2005).

We next sought to determine the Nap1-binding regions in the cytoplasmic domain of OL-pc. We constructed a series of GST–OL-pc fusion proteins containing various deletions (Fig. 1 C, top) and performed pull-down assays with them. The results showed that the region from aa 987 to 1,025 was essential for pulling down not only Nap1 but also CYFIP1 (Sra-1), WAVE1, and Abi-1 (Fig. 1 C, bottom). This region was therefore defined as the NBS. To confirm these results, we constructed OL-pcΔNBS, in which the NBS was deleted, and transfected U251 cells with HA-tagged OL-pcΔNBS or full-length OL-pc (OL-pc). Immunoprecipitates of these constructs showed that Nap1 was copurified only with the full-length construct (Fig. 1 D).

OL-pc recruits NAP1 and WAVE1 to cell–cell contacts

To study the biological role of the OL-pc–Nap1 complex, we transfected U251 cells with cDNAs for OL-pc and OL-pcΔNBS and isolated their stable transfectant lines. Each line was a mixture of uncloned transfectants, which allowed us to avoid observing clone-specific phenotypes. Despite the description in the GEO DataSets (National Center for Biotechnology Information) that OL-pc mRNA is expressed in the U251 line, we did not detect any endogenous OL-pc protein in it. In low cell density cultures, U251 cells were highly motile, exhibiting a polarized fanlike shape with lamellipodia at the leading edge (Video 1, available at http://www.jcb.org/cgi/content/full/jcb.200802069/DC1). When these cells had collided, they formed transient contacts, although they soon became separated from one another as a result of the high locomotive activities. In higher densities, they more stably contacted each other. Irrespective of the cell densities, the exogenous OL-pc and OL-pcΔNBS were always concentrated at cell–cell contact sites (Fig. 2 A). These molecules were also detectable in the lamellipodial regions, where they were well colocalized with actin fibers (Fig. 2 A, right).

these cells. Comparison of each experimental group to the control one shows no significant difference (n.s.) at a significance level of $\alpha = 0.05$. P = 0.13 for OL-pc, and P = 0.27 for OL-pcΔNBS. *n* = 38, 49, and 39 for control, OL-pc, and OL-pcΔNBS, respectively. (right) Directionality in cell migration defined by the ratio of the direct distance between the starting and ending points for migration to the total track distance. No difference was observed between control (*n* = 38) and OL-pc–expressing cells (P = 0.28; *n* = 47) or OL-pcΔNBS–expressing cells (P = 0.22; *n* = 36). Error bars represent SEM. (B) Time-lapse images of cells making contact with others in low density cultures and their drawings. The numbers denote the time elapsed (in minutes). Arrows indicate the directions of cell movement together with the highest lamellipodial activity. Control cells or OL-pcΔNBS transfectants temporarily move together in the same direction when they meet others, whereas OL-pc transfectants never display such coordination. Also see Video 1 and Video 2 (available at http://www.jcb.org/cgi/content/full/jcb.200802069/DC1) for the control and OL-pc transfectant samples, respectively. Bars: (A) 200 μm; (B) 50 μm.

We then compared the distributions of OL-pc and Nap1 in low or high density cultures. In control U251 cells transfected with vain vectors, Nap1 was highly concentrated along the lamellipodia (Fig. 2 A). OL-pc transfectants also displayed Nap1 localized on the lamellipodia. These lamellipodial Nap1 signals overlapped with OL-pc ones, but their distribution patterns were not exactly identical. Most intriguingly, in the OL-pc transfectants, Nap1 also became detectable at cell–cell contact sites together with OL-pc signals, in contrast with no such signals in the control cells (Fig. 2 A). However, detection of these junctional Nap1 molecules was sometimes hampered by diffuse immunoreactive signals for Nap1 in the cytoplasm. To improve detection sensitivity, we extracted cells with 0.5% Triton X-100 for 10 min before fixation, which removed soluble proteins but allowed retention of the cytoskeletal structures. After this treatment, Nap1 immunoreactive signals were reduced at the lamellipodia and cytoplasm; nevertheless, Nap1 was retained at cell–cell contacts (Fig. 2 B). These insoluble Nap1 colocalized with OL-pc, which was also resistant to the detergent extraction.

In the OL-pcΔNBS transfectants, Nap1 was also localized along the lamellipodia, overlapping with OL-pcΔNBS (Fig. 2 A). Because these two molecules did not interact with each other biochemically (Fig. 1), Nap1 was likely distributed to the lamellipodia in an OL-pc–independent way. More importantly, in the OL-pcΔNBS transfectants, Nap1 was not localized at cell–cell contact sites (Fig. 2, A and B). These observations suggest that the OL-pc accumulation at cell–cell contacts resulted in the recruitment of Nap1 to the same sites, which was otherwise present only on the lamellipodia, at least in the cell line used here.

Then, we examined the distribution of WAVE1. Because antibodies useful for immunostaining of this molecule were not available, we transiently transfected the aforementioned cells with a GFP-conjugated WAVE1. The behavior of WAVE1 was similar to that of Nap1: in control U251 cells, WAVE1 was concentrated mainly on the lamellipodia, whereas it became localized at cell junctions when OL-pc was coexpressed (Fig. 2 C). OL-pcΔNBS coexpression had no such effects. These findings are in accord with the observation that Nap1 and WAVE behave together, forming a complex (Ibarra et al., 2005). On the other hand, the distribution of Arp2/3 complex, which is known to be downstream of the Nap1–WAVE signals, was unique, as revealed by immunostaining for ARPC2 (Arp2/3 complex 34-kD subunit), a component of the Arp2/3 complex (Robinson et al., 2001). In control U251 cells, ARPC2 was localized along the leading edge of cells, with additional irregular signals at cell–cell contacts. However, OL-pc expression did not particularly change this localization pattern. Furthermore, we never observed specific colocalization of OL-pc and ARPC2 at cell–cell contact regions, and this was also the case for OL-pcΔNBS (Fig. S1, available at http://www.jcb.org/cgi/content/full/jcb.200802069/DC1), suggesting that the Arp2/3 complex was not interacting with OL-pc.

OL-pc has no effect on the migration of isolated cells but up-regulates cell motility within colonies

Nap1 and its associated components are known to regulate cell motility. Therefore, we examined whether OL-pc expression had any effect on cell migration by comparing the parent cells with their transfectants. Cells were plated at low densities to allow their free migration, and their movement was then recorded by time-lapse microscopy. Analysis of the video images did not show any difference in migration speed between the control and OL-pc–transfected cells (Fig. 3 A). We also measured the directionality of cell migration, which was defined previously (Pankov et al., 2005), but could not find any difference in this parameter either between these cells (Fig. 3 A). Careful observation of the videos, however, made us aware that these cells were different in their contacting behavior. When the parent U251 cells made contact with each other, their membrane ruffling was suppressed at the contact sites, and these contact sites as well as the overall polarity of cells, including the lamellipodial directions, were transiently maintained until detachment (Fig. 3 B and Video 1). OL-pc–expressing cells also formed transient contacts; however, these cells in contact randomly moved relative to each other, rapidly changing the lamellipodial positions, suggesting that their peripheral motile activity was not properly controlled by cell–cell contacts (Fig. 3 B and Video 2, available at http://www.jcb.org/cgi/content/full/jcb.200802069/DC1). The association pattern of OL-pcΔNBS–expressing cells was similar to that of the control cells, indicating that the aforementioned action of OL-pc required its binding to Nap1.

Under the aforementioned low density culture conditions, the formation of cell–cell contacts was sporadic. To examine the effects of OL-pc expression on the behavior of contacting cells in a quantitative way, we prepared confluent cultures in which fluorescence-labeled and nonlabeled cells were mixed in a 1:10 ratio and then traced the labeled cells by time-lapse recording, as described previously (Joslin et al., 2007). The results showed that OL-pc–expressing cells gave longer tracks than the control cells on average (Fig. 4), suggesting that OL-pc expression accelerated the migration of cells under this specific condition. On the other hand, OL-pcΔNBS–expressing cells exhibited rather shorter migration tracks than the controls (Fig. 4 B).

As another way to measure the cell behavior, we conducted a wound-healing assay in which cell migration was stimulated under the conditions in which cells were in contact with each other. When wounds had been produced by cell scraping of confluent cultures, the cells located around the wound edges became polarized so as to migrate toward the open space within 10 min. In control cultures, cells occupying the front line of the wound were arranged in parallel and moved together, maintaining their mutual contacts in which individual cells kept roughly a similar pace, suggesting that their movements were coordinated (Fig. 5 A, control; and Video 3, available at http://www.jcb.org/cgi/content/full/jcb.200802069/DC1). At their lateral contact sites, the membrane ruffling was prohibited, indicating that the contact inhibition of movement was also operating in this system. On the other hand, the movement of OL-pc–expressing cells was rarely coordinated: they dynamically changed their positions relative to those of their neighbors during translocation (Fig. 5 A, OL-pc; and Video 4), as was quantified by defining the farthest and nearest indices (Fig. 5 D). Many of them abruptly moved out of the original positions, leaving their neighbors behind, which resulted in the positioning of themselves at the front-most edge of the wound. This type of

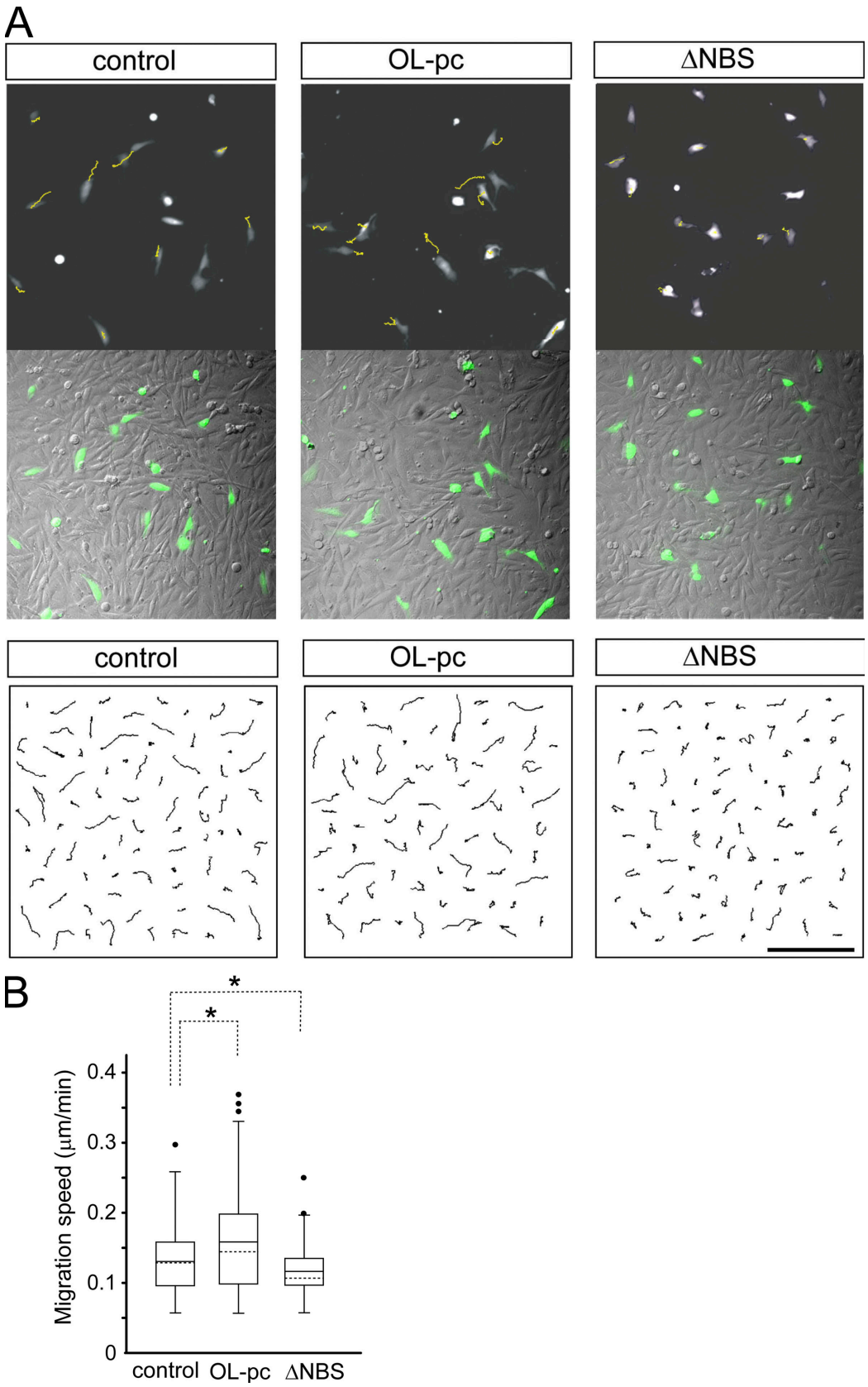

Figure 4. **Migration of cells in confluent monolayers.** (A) Migration of fluorescence-labeled cells cocultured with nonlabeled cells. Time-lapse images were acquired at 9-min intervals for 6 h. Tracks of some labeled cells, which are shown in yellow, are overlaid with the last frame shot of a representative video in the top panels, where phase-contrast images are also shown. Representative tracks are collected in the bottom panels. (B) Statistic analysis of the instantaneous velocities of cells. Comparison of each experimental group with the control cells ($n = 76$) shows a significant difference for OL-pc (*, $P < 0.05$; $n = 63$) as well as for OL-pcΔNBS (*, $P < 0.05$; $n = 76$). Bar, 200 μm.

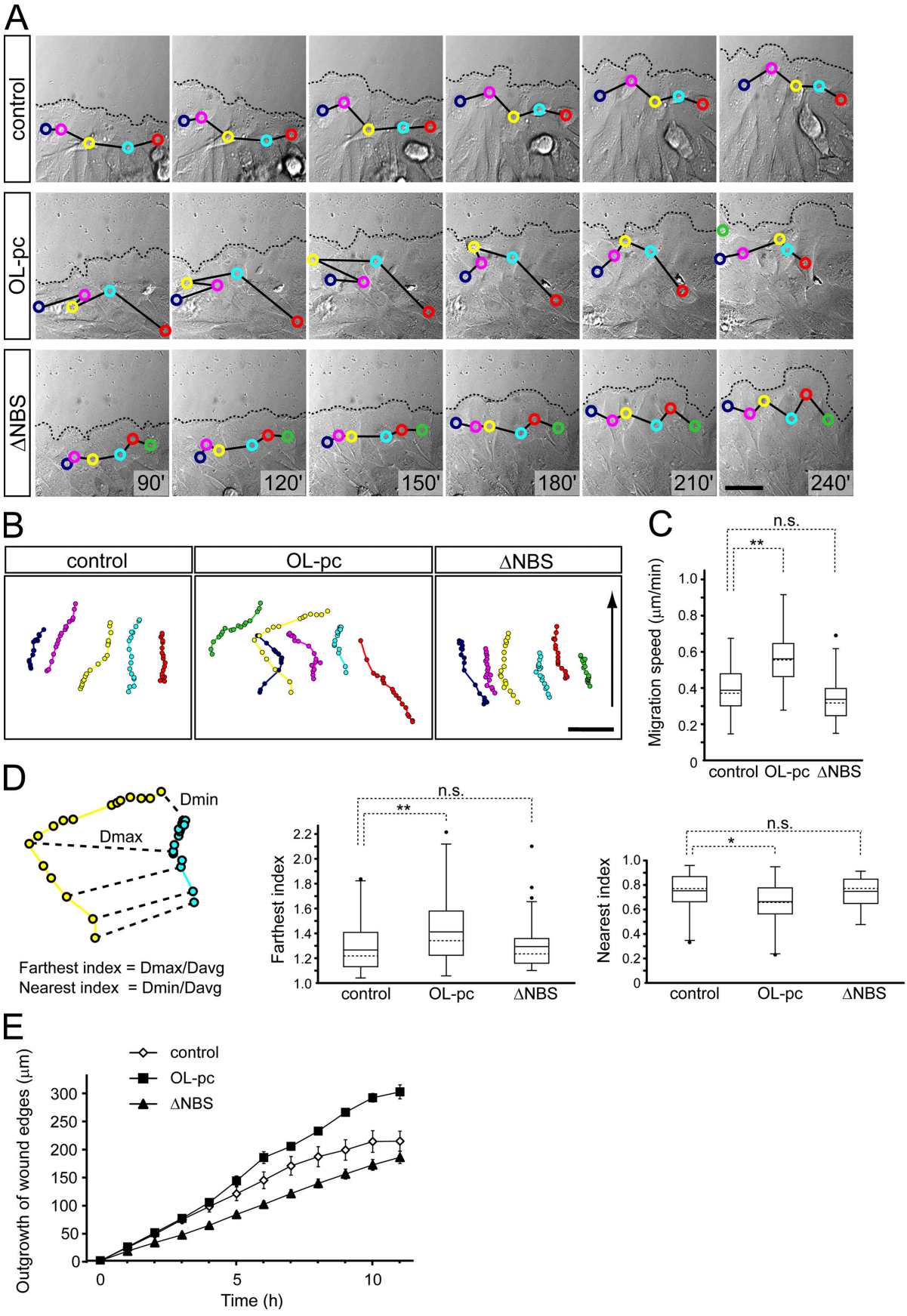

Figure 5. **OL-pc expression accelerates cell movement in wound healing.** (A) Confluent cell layers were wounded by cell scraping, and the wounded edges were immediately processed for time-lapse recording. Phase-contrast images were taken for 4 h at 3-min intervals. At the end of the recording,

uncoordinated movement was also detectable in the control cell cultures, but its frequency was greatly increased in the OL-pc–expressing cells.

Tracing the movement of individual cells confirmed the aforementioned observations: control cells moved with a relatively constant speed, whereas OL-pc–expressing ones intermittently increased their speed and then decreased it back to the regular speed (Fig. 5 B); as a whole, the latter moved faster than the former (Fig. 5 C). As a result of these differences, the cell colonies with OL-pc spread faster than those without it (Fig. 5 E). On the other hand, OL-pcΔNBS did not show any accelerated cell migration (Fig. 5, A–C; ΔNBS; and Video 5, available at http://www.jcb.org/cgi/content/full/jcb.200802069/DC1), and these constructs actually rather suppressed colony spreading (Fig. 5 E), as observed in the experiments shown in Fig. 4, suggesting that the undeleted portions of the cytoplasmic domain in OL-pcΔNBS might have uncharacterized functions to suppress cell motility. To summarize, OL-pc did not alter the motility of solitary U251 cells but accelerated the translocation of cells that were in contact with each other, thus suggesting that OL-pc acted on cell motility via cell–cell contacts, where this molecule was concentrated.

Requirement of Nap1 and WAVE1 for OL-pc action

To test whether Nap1 and WAVE1, which associated with OL-pc, were involved in the aforementioned activity of OL-pc, we looked at the effects of RNAi-mediated depletion of these proteins. siRNAs designed for Nap1 and WAVE1 significantly down-regulated the expression of the respective molecules, and control siRNA had no such effects. In addition, the depletion of Nap1 was accompanied by a decrease in the WAVE1 level (Fig. S2, available at http://www.jcb.org/cgi/content/full/jcb.200802069/DC1), suggesting that the stability of WAVE1 was dependent on Nap1. Knockdown of Nap1 in control U251 or OL-pc transfectants resulted in the suppression of lamellipodial formation as reported previously (Steffen et al., 2004), and that of WAVE1 expression also suppressed formation of their polarized lamellipodia (Fig. S3).

Next, we compared the behavior of control and OL-pc transfectants from which Nap1 or WAVE1 was depleted in the wound-healing assay. At the wound edges of Nap1-depleted control U251 cells, these cells appeared more slender than their Nap1-positive counterparts (Fig. S4, available at http://www.jcb.org/cgi/content/full/jcb.200802069/DC1), and, despite their defective lamellipodia formation, they migrated actively (Fig. 6 A and Video 6). When their migration was compared with that of Nap1-depleted OL-pc transfectants, the latter migrated slightly faster than the former (Fig. 6 B and Video 7). However, these Nap1-depleted OL-pc transfectants did not display the uncoordinated migration that was unique to the Nap1-positive OL-pc transfectants but did migrate in a pattern similar to control cells (Fig. 6, A and C). Thus, the migration profile became indistinguishable between the cells with and without OL-pc, except for the migration speed, in the absence of Nap1. WAVE1 depletion produced similar results to that of Nap1, although the overall migration speed of U251 cells was greatly reduced (Fig. 6 and Fig. S4). These results suggest that OL-pc required Nap1 and WAVE1 in inducing the uncoordinated cell movement, although it did not require them for simple enhancement of cell migration.

OL-pc perturbs actin organization and cadherin-based junctions

Because Nap1 associating with OL-pc is an actin regulator, we asked whether any changes were induced in actin assembly after OL-pc expression. The overall actin-staining pattern was too complex to compare between these cells. However, we found significant differences in the organization of actin-associated cell junctions, where classical cadherins were localized, between the presence and absence of OL-pc. U251 cells expressed N-cadherin, and this classical cadherin was lineally arranged along cell–cell boundaries, and a similar localization pattern for N-cadherin was observed in OL-pcΔNBS transfectants. Double immunostaining for N-cadherin and OL-pcΔNBS showed that although OL-pcΔNBS was distributed throughout the cell–cell contact regions, N-cadherin tended to be condensed along the apical-most portion of the junctions (Fig. 7 A), as generally seen in epithelial cells. In OL-pc transfectants, on the other hand, N-cadherin was detected as streaklike signals spread over the OL-pc–positive areas, oriented perpendicularly to the cell borders (Fig. 7 A). Cadherin-associated catenins, such as α-catenin, showed a localization pattern similar to that of N-cadherin in each transfectant.

Double staining for N-cadherin and F-actin showed that in control and OL-pcΔNBS transfectants, diffuse F-actin signals were localized parallel to cell–cell boundaries, colocalizing with

individual cells located along the front of cell sheets were marked with colored circles over their nuclear positions, and the same cells were tracked back to earlier time points. At each time point, the circles were connected with lines in a fixed order. Dashed lines represent wound edges. The numbers denote the time elapsed (in minutes). Control and OL-pcΔNBS transfectants roughly maintain their relative positions during migration, whereas OL-pc transfectants irregularly change their spatial relations with neighbors (e.g., the cell marked with the red circle at the right jumped out to the front position from an initially deep site). Videos 3–5 are available at http://www.jcb.org/cgi/content/full/jcb.200802069/DC1. (B) Migration track of individual cells marked with different colors in A, with cell position plotted at 9-min intervals. The arrow indicates the direction of wound healing. Abrupt acceleration of movement is most frequently seen in OL-pc transfectants. (C) Statistical analysis of the instantaneous velocities of cells during wound healing. Comparison of each experimental group with the control cells ($n = 38$) shows a significant difference for OL-pc (**, $P < 0.0005$; $n = 51$) but not for OL-pcΔNBS ($P = 0.70$; $n = 41$). (D) Changes in the positions of cells relative to those of their neighbors during migration. At the end of recording (at 240 min after scraping), all cells at the wound edges were marked as in A, and their migration track was drawn as in B. Choosing a pair of cells located next to each other at the 240-min point, the distances between their nuclei at earlier time points were measured at 15-min intervals, and their means as well as the farthest and nearest distances were obtained. The farthest and nearest indices were defined as the ratio of the farthest (Dmax) and nearest (Dmin) distance to the average distance (Davg), respectively, as illustrated in the left panel. The farthest index for OL-pc transfectants is significantly larger (**, $P < 0.0005$; $n = 77$) than that for the control cells ($n = 58$), whereas that for OL-pcΔNBS transfectants ($P = 0.39$; $n = 63$) is not. Likewise, the nearest index for OL-pc transfectants is significantly smaller (*, $P < 0.005$) than that for the controls, whereas that for OL-pcΔNBS (n.s.; $P = 0.87$) is not. (E) Changes in the mean distance (±SEM [error bars]) of the migrating wound edges from their starting position during a long incubation period up to 11 h. $n = 12$ for all samples. Bar, 50 μm.

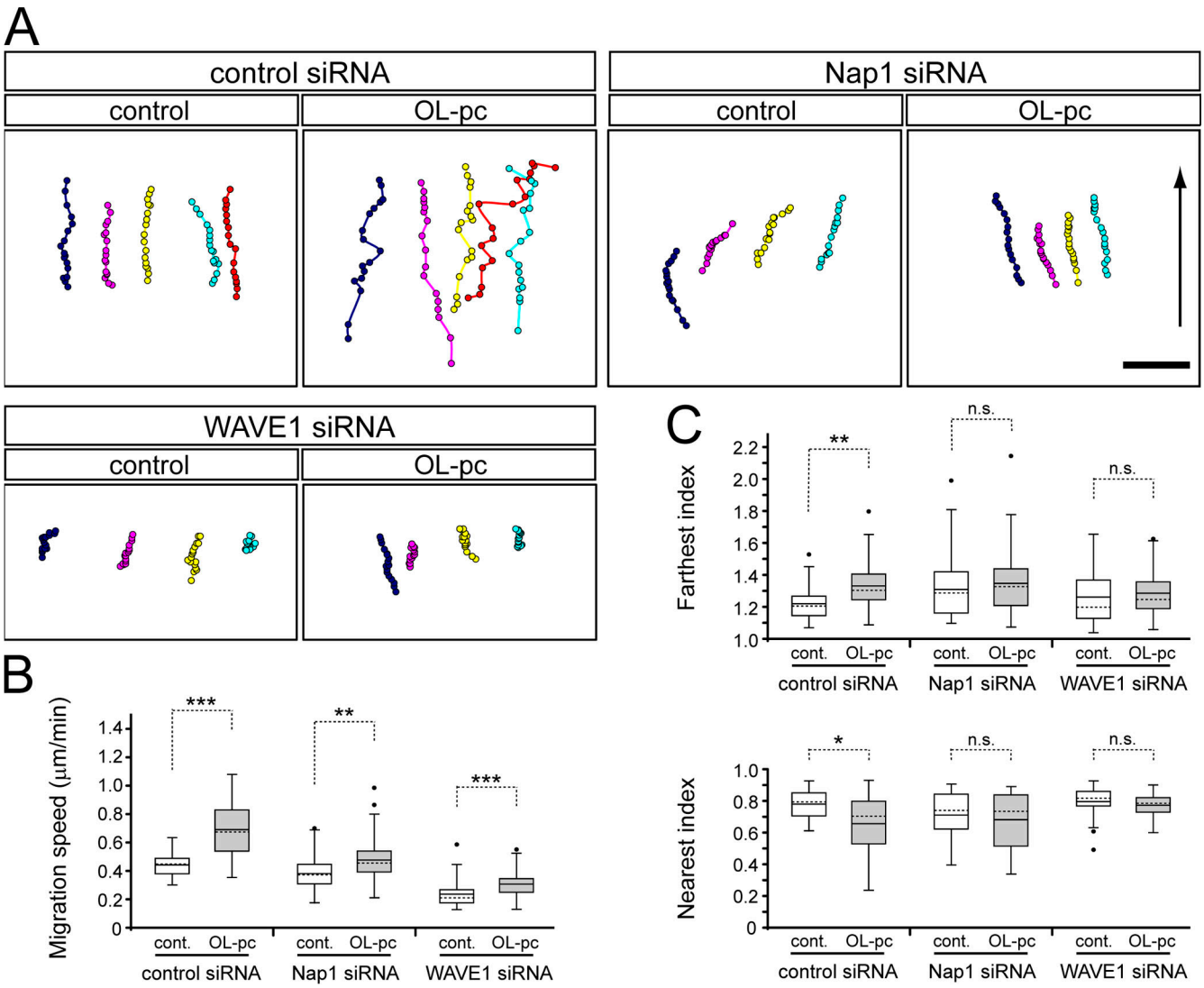

Figure 6. **Nap1 and WAVE1 are required for OL-pc function.** (A) Control U251 cells and OL-pc-HA transfectants were treated with control, Nap1, or WAVE1 siRNA, and their migration pattern during wound healing was analyzed as described in Fig. 5. See Fig. S4 for the original photographs of these cells. Also see Videos 6 and 7 (available at http://www.jcb.org/cgi/content/full/jcb.200802069/DC1) for the videos of Nap1-depleted cells without and with OL-pc, respectively. The arrow indicates the direction of wound healing. (B) Quantification of the instantaneous velocities of those cells. n = 31 and 29 for control and OL-pc transfectants with control siRNA, respectively; n = 40 for both control and OL-pc transfectants with Nap1 siRNA; n = 29 and 34 for control and OL-pc transfectants, respectively, treated with WAVE1 siRNA. **, P < 0.005; ***, P < 0.0005. (C) The farthest and nearest indices obtained as in Fig. 5 D. n = 23 and 22 for control and OL-pc transfectants with control siRNA, respectively; n = 30 for both control and OL-pc transfectants with Nap1 RNAi; n = 23 and 24 for control and OL-pc transfectants with WAVE1 siRNA, respectively. *, P < 0.05; **, P < 0.005. n.s., P = 0.35 and 0.44 for Nap1 siRNA–treated cells and P = 0.83 and 0.06 for WAVE1 siRNA–treated cells for the farthest and nearest indices, respectively. Bar, 50 μm.

N-cadherin, whereas in OL-pc transfectants, the junctional F-actin stretched over cell–cell contact zones, colocalizing with the streaklike N-cadherin signals (Fig. 7 B). Importantly, the actin signals associated with N-cadherin were continuous with the stress fiber–like actin fibers, resembling radial actins, which had been previously shown to terminate at early cadherin-mediated adherens junctions in keratinocytes (Vaezi et al., 2002). In contrast, N-cadherin–associated F-actins in control or OL-pcΔNBS transfectants were isolated from the major cytoplasmic actin fibers. In all of these cells, the total level of N-cadherin was similar (Fig. S2). To investigate the dynamic aspects of N-cadherin and F-actin accumulation at cell–cell contacts, we conducted Ca^{2+}-switch assays by treating cells with 1 mM EGTA to disrupt cadherin-mediated junctions and adding normal medium to the culture. N-cadherin was restored to cell–cell boundaries within 15 min, together with OL-pc or OL-pcΔNBS in the case of their transfectants. Even at these early cell–cell contacts, N-cadherin and F-actin exhibited the localization patterns characteristic of the control, OL-pc, and OL-pcΔNBS transfectants (Fig. 7 C), indicating that the OL-pc–dependent behavior of N-cadherin and F-actin was tightly linked.

As an attempt to characterize the aforementioned actin organization unique to OL-pc transfectants, we treated cells with cytochalasin D. This treatment eliminated most of the major actin fibers in the cells but left the junctional cortical actins intact. After this treatment, the distribution of N-cadherin–associated actins became indistinguishable between OL-pc and OL-pcΔNBS transfectants or control cells (Fig. 7 D). Thus, the cytochalasin D

treatment abolished the effects of OL-pc–dependent reorganization of junctional actins, suggesting that OL-pc expression primarily altered the actin polymerization states. We also examined the N-cadherin and actin distributions in Nap1 or WAVE1 siRNA–treated cells. In these cells, the OL-pc–dependent streaklike localization of N-cadherin was diminished, being converted to a pattern similar to that seen in control cells (Fig. 7 E), supporting the idea that Nap1 and WAVE were working together with OL-pc.

N-cadherin depletion mimics OL-pc expression

The altered N-cadherin distribution, as shown in Fig. 7, might have been involved in the migration behavior specific to the OL-pc transfectants. To test this possibility, we looked at the effects of RNAi-mediated depletion of N-cadherin (Fig. S2) on cell migration by using the wound-healing assay. Our results showed that N-cadherin–depleted cells, whether OL-pc was expressed or not, became similar to OL-pc–expressing cells in terms of their migratory behavior (i.e., they showed an accelerated movement; Figs. 8 and S4), indicating that N-cadherin removal was sufficient to induce the phenotypes seen by OL-pc expression. To check whether cadherin activity was altered by OL-pc expression, we dissociated control and OL-pc transfectants by using the classic trypsin-Ca^{2+} treatment protocol, by which cadherins on the cell surface are preserved (Takeichi, 1977), and measured their aggregation rate in suspension cultures. However, we did not find any significant difference in their aggregating abilities (unpublished data). These results suggest that the role of OL-pc is not to interfere with cadherin-dependent cell adhesion but to perturb other cadherin-mediated signaling processes.

Discussion

A unique feature of the cadherin superfamily members is that they undergo homophilic interactions via their extracellular domains. This form of interaction is used for the physical associations of cells; this is particularly the case for classical and desmosomal cadherins and for some other members of the superfamily (Kazmierczak et al., 2007). However, these homophilic interactions can be used not only for cell–cell adhesion but also for intercellular signaling; in fact, *Drosophila* Flamingo and its vertebrate homologues, which are members of the cadherin subfamily, have been shown to act as regulators of planar cell polarity or as signals for homotypic repulsion between cells (Takeichi, 2007). Our present results suggest that OL-pc also functions as an intercellular signaling mediator.

We found that OL-pc was coprecipitated with components of the Nap1–WAVE complex (Stradal and Scita, 2006). Our results further suggested that Nap1 was the primary element to interact with OL-pc among the components of the complex. Immunostaining experiments showed that in control U251 cells, Nap1 or WAVE1 was localized exclusively on the lamellipodia, except for other diffuse cytoplasmic signals. However, OL-pc expression recruited these molecules to cell–cell contact sites. This recruitment most likely resulted from the autonomous concentration of OL-pc molecules into cell junctions as a result of their homophilic interaction. On the other hand, OL-pc was also detectable on lamellipodia, whose signals partly colocalized with those of Nap1. However, OL-pcΔNBS, not having the Nap1-binding region, also showed similar lamellipodial localization, suggesting that the association of OL-pc with lamellipodia did not depend on its interaction with Nap1. Both OL-pc and OL-pcΔNBS colocalized with actin fibers at the lamellipodia, suggesting the possibility that they may be able to associate with F-actin by using the non-NBS portion of their cytoplasmic domain. Although the OL-pc localized on lamellipodia may have some biological roles, in the present experiments, we focused on the NBS-dependent functions of OL-pc.

The Nap1–WAVE complex is known to enhance lamellipodia formation and, in turn, cell migration. It is therefore expected that when this complex has been recruited to cell junctions, even the junction-forming cell peripheries might have acquired lamellipodium-like activities. Indeed, we found that the motile behavior of cells was altered by OL-pc when they were in contact with one another. In low density cultures of control U251 cells, when they had transiently contacted each other, their membrane ruffling was suppressed at their contact sites, but this suppression did not affect their overall polarity, including the lamellipodial sites. On the other hand, OL-pc–expressing cells rapidly changed their association pattern with their partners, actively altering lamellipodial directions. These observations suggest that although the wild-type U251 cells have the ability to control their lamellipodial activity upon their contacts, this ability was perturbed by OL-pc expression. This notion was supported by the finding that cell movement was accelerated within cell colonies by OL-pc expression. Similar differences in cell behavior were also observed for cells undergoing wound healing: contrasted with the coordinated migration of control cells at wound edges, the behavior of OL-pc–expressing cells was uncooperative. For example, their migration was sporadically accelerated in the presence of neighbors. All of these findings support the idea that the OL-pc–Nap1–WAVE1 complex stimulated cell motility by localizing at cell–cell contact sites.

The clearest morphological differences between the cells with and without OL-pc were seen in terms of actin organization at the N-cadherin–based cell junctions: in the absence of OL-pc or its NBS, N-cadherin and F-actin, which are the key partners required for organization of the adherens junction (Mege et al., 2006), were localized parallel to cell–cell interfaces. In contrast, in the presence of OL-pc, they were rearranged to stretch perpendicularly to the cell boundaries, becoming linked with radial actin fibers. However, this unique OL-pc–dependent reorganization of F-actin and N-cadherin was abolished by treatment with cytochalasin D, whose direct targets are the actin filaments. These findings suggest the possibility that the OL-pc–Nap1–WAVE complex primarily remodels F-actin assembly at cell–cell contact sites and that this change, in turn, alters the adherens junctions, as adherens junction formation is known to depend on F-actin organization (Mege et al., 2006; Abe and Takeichi, 2008).

With regard to the signaling systems downstream of the OL-pc–associated Nap1, it seems likely that Nap1 and WAVE1 act together, as is well established (Blagg and Insall, 2004) and supported by the observation that the RNAi-mediated removal of these two molecules abolished OL-pc–dependent phenotypes

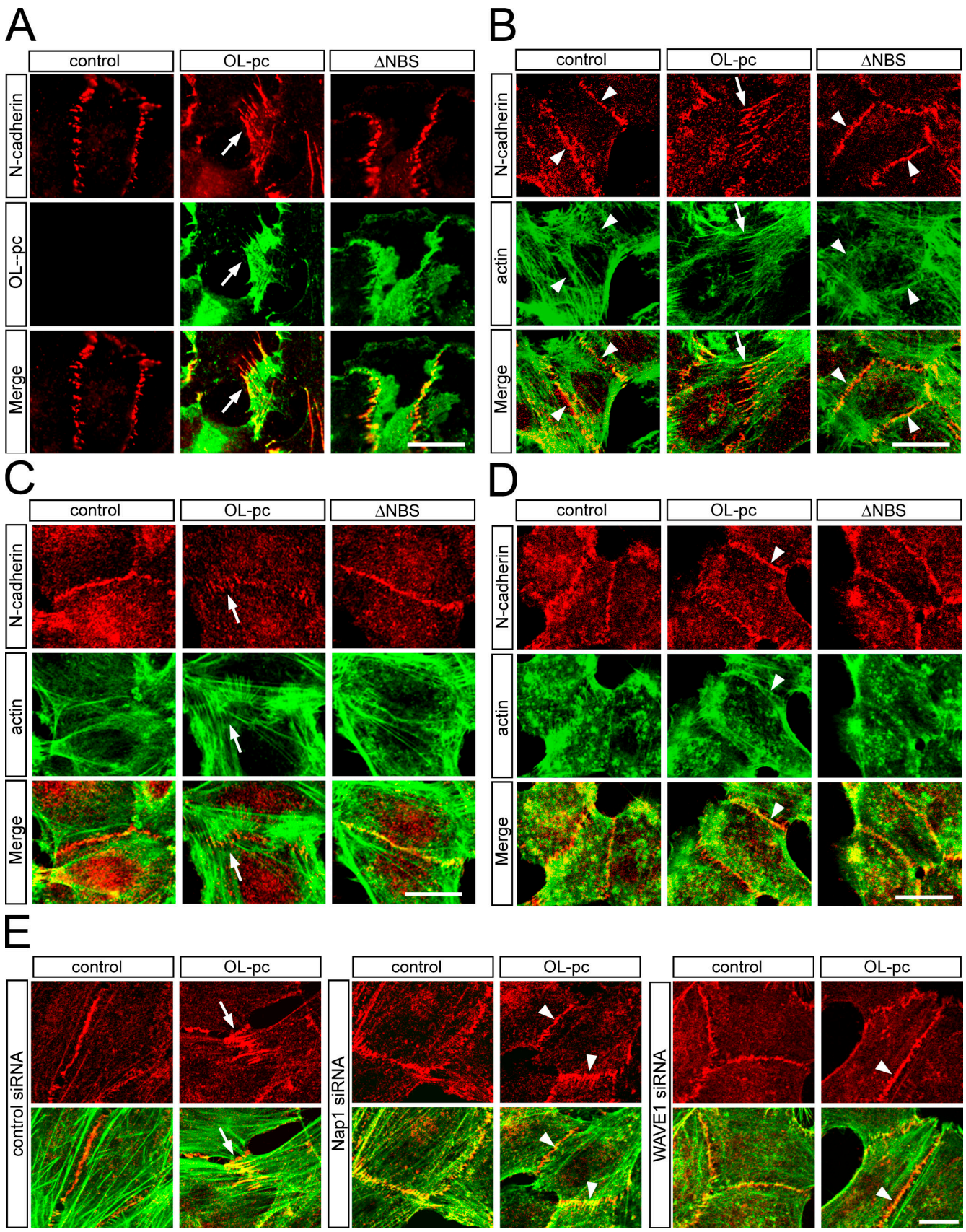

Figure 7. **OL-pc alters the distribution of junctional F-actin and N-cadherin.** (A) Double immunostaining for N-cadherin and HA tag. N-cadherin signals are linearly arranged along the cell borders in control and OL-pcΔNBS transfectants. N-cadherin is concentrated along the apical-most region of the obliquely formed cell–cell contacts, which was identified by differential focusing. In OL-pc transfectants, however, N-cadherin assumes a streaklike distribution over the OL-pc–positive cell–cell contact areas (arrows). (B) Double immunostaining for N-cadherin and F-actin. In control cells or OL-pcΔNBS transfectants,

in a similar fashion. On the other hand, our results imply that the Arp2/3 complex, the classic target of WAVE, was unlikely to be involved in the OL-pc signaling system, as this complex did not show any colocalization with OL-pc at cell junctions. It is probable that the OL-pc–associated WAVE1 may use some other signaling system rather than Arp2/3; in fact, the presence of Arp2/3-independent pathways for WAVE signaling was indeed suggested in a previous study (Sasaki et al., 2000). Our results also suggest that OL-pc had some functions independent of the Nap1–WAVE complex. For example, when Nap1 or WAVE1 had been depleted, OL-pc–positive cells still migrated faster than OL-pc–negative cells. Furthermore, the cell migration speed in confluent cultures or during wound healing was rather reduced by OL-pcΔNBS expression. It is very likely that other regions on the OL-pc cytoplasmic domain than the NBSs bear uncharacterized biological functions, which need to be identified by future studies.

How, then, did the OL-pc–Nap1 complex affect cell migratory behavior? As discussed in the previous sections, it might have activated the motile machinery at cell–cell contact sites via F-actin remodeling, which was otherwise quiescent, and this could be a mechanism to explain the OL-pc–dependent cell behavior. Interestingly, the behavior of OL-pc–expressing cells was mimicked by N-cadherin depletion. Thus, it should be recalled that the cadherin-based cell junctions are required for contact inhibition of cell movement (Chen and Obrink, 1991; Bracke et al., 1997; Huttenlocher et al., 1998). Thus, the aforementioned proposed role of OL-pc might have been elicited through an alteration of N-cadherin functions. For example, we can infer the following sequence of OL-pc action: OL-pc first altered F-actin organization, which caused N-cadherin redistribution, and the redistributed N-cadherin molecules lost the ability to induce contact inhibition, although they did not lose the cell adhesion function, as shown in the present results. Cells, which are less contact inhibited, would display accelerated movement within their monolayers, as observed in this study. It is noteworthy that paraxial protocadherin inhibits the activity of classical cadherins (Chen and Gumbiner, 2006), and arcadlin enhances endocytosis of N-cadherin (Yasuda et al., 2007). These protocadherins share clusters of conserved cytoplasmic sequences with OL-pc (Redies et al., 2005; Vanhalst et al., 2005), suggesting the possibility that they may have conserved biological functions that affect the classical cadherin system.

Our previous analysis using OL-pc knockout mice revealed that striatal axons could not normally extend not only in vivo but also in vitro, when the OL-pc gene had been removed (Uemura et al., 2007). When striatal neurons are dissociated into single cells and cultured in vitro, they do normally elongate irrespective of the presence or absence of OL-pc (unpublished data), suggesting that the ability of elongation is indistinguishable between wide-type and mutant axons. Notably, in vivo, OL-pc–deficient striatal axons clumped together at the stalled points, which is in contrast with the dispersed arrangements of growing normal axons, suggesting that some signals to repel the axons from each other are missing in the mutants. Immunostaining experiments revealed that OL-pc was distributed along axons, particularly concentrated in the growth cones (Uemura et al., 2007), and Nap1 was localized in a similar pattern (unpublished data). During the course of axon elongation, these growth cones may laterally touch each other as they migrate, forming a fascicle. In such occasions, the homophilic interactions could occur between the OL-pc–Nap1 complexes localized on the contacting growth cones, and they may generate signals to facilitate their migration (for example, by activating the cell locomotive machinery localized at the cell periphery). In conclusion, our results disclosed a novel regulatory mechanism for cell migration, one that operates specifically at the homotypic cell–cell contact sites.

Materials and methods

Plasmids

Mouse OL-pc full-length cDNA was described previously (Nakao et al., 2005). A partial cDNA clone of mouse Nap1 (IMAGE: 3488144) and a full-length clone of mouse CYFIP-2 (NCBI: AK030397) were obtained from the Mammalian Gene Collection (National Institutes of Health, Bethesda, MD) and FANTOM2 clone (Institute of Physical and Chemical Research, Kobe, Japan), respectively, via the Genome Resource/Analysis Laboratory in the RIKEN Center for Developmental Biology. For obtaining the full-length Nap1, the 5′ sequence was amplified by PCR using Mouse Brain Marathon-Ready cDNA (BD Biosciences) as a template. The 5′ fragment was subsequently inserted into the original Mammalian Gene Collection clone. To generate HA-, Myc-, or FLAG-tagged proteins, we subcloned cDNAs encoding the full-length OL-pc, an OL-pc mutant comprising aa 1–985, Nap1, and CYFIP-2 into pCA-sal-HA (Otani et al., 2006), pCA-sal-Myc (constructed by S.C. Suzuki), or pCA-sal-FLAG vector (constructed by T. Ichii). For the generation of OL-pcΔNBS-HA, a C-terminal portion of OL-pc comprising aa 1,027–1,041 was inserted into the aforementioned HA-tagged OL-pc mutant. The resultant OL-pc-HA and OL-pcΔNBS-HA were subcloned into the pCA-Sal-IRES-neomycin vector (Kametani and Takeichi, 2007) to obtain stable expression vectors. The WAVE1 expression vector cloned into pEGFP (Clontech Laboratories, Inc.) was provided by T. Takenawa (Kobe University, Kobe, Japan).

Cell culture and transfection

U251 human astrocytoma cells were cultured on collagen-coated dishes (Iwaki) in a 1:1 mixture of DME and Ham's F12 (Wako) supplemented with 10% FCS (abbreviated as DH10). Cells were transfected with various expression vectors by use of TransIT-LT1 Transfection Reagents (Mirus) or an electroporation system (Amaxa). For obtaining stable transfectants, transfected cells were selected with 500 μg/ml G418 for 2–3 wk and maintained as uncloned populations, in which we confirmed that >90% of the cells in each culture expressed the transgene. Cytochalasin D (EMD) was added to the culture medium at a final concentration of 0.4 μg/ml, and the cells were fixed after 30 min. For calcium-switch assays, cell layers were incubated for 15 min at 37°C in a Hepes-buffered saline containing 1 mM EGTA and 1 mM $MgCl_2$. Then, the saline was replaced with prewarmed DH10, and the cells were maintained in it until examined.

N-cadherin colocalizes with nonfibrous F-actin signals (arrowheads), whereas in OL-pc transfectants, N-cadherin is associated with the terminals of radial actin fibers (arrows). (C) Ca^{2+}-switch experiment. Cells were preincubated with 1 mM EGTA to inactivate cadherins and were incubated in normal culture medium for 15 min. Double immunostaining for N-cadherin and F-actin shows that their distribution patterns unique to each transfectants are already observable at this time point (arrows). (D) Cells were treated with DMSO (control) or 0.4 μg/ml cytochalasin D for 30 min at 37°C and were stained for N-cadherin and F-actin. The unique distributions of N-cadherin in OL-pc transfectants were abolished by cytochalasin D (arrowheads). (E) Control and OL-pc-HA transfectants were treated with control, Nap1, or WAVE1 siRNA and double stained for N-cadherin (red) and F-actin (green; shown in each of the merged images). Arrows point to OL-pc transfectant-specific distribution of N-cadherin, and arrowheads indicate the restored distribution of N-cadherin. All images were taken with a confocal microscope. Bars, 10 μm.

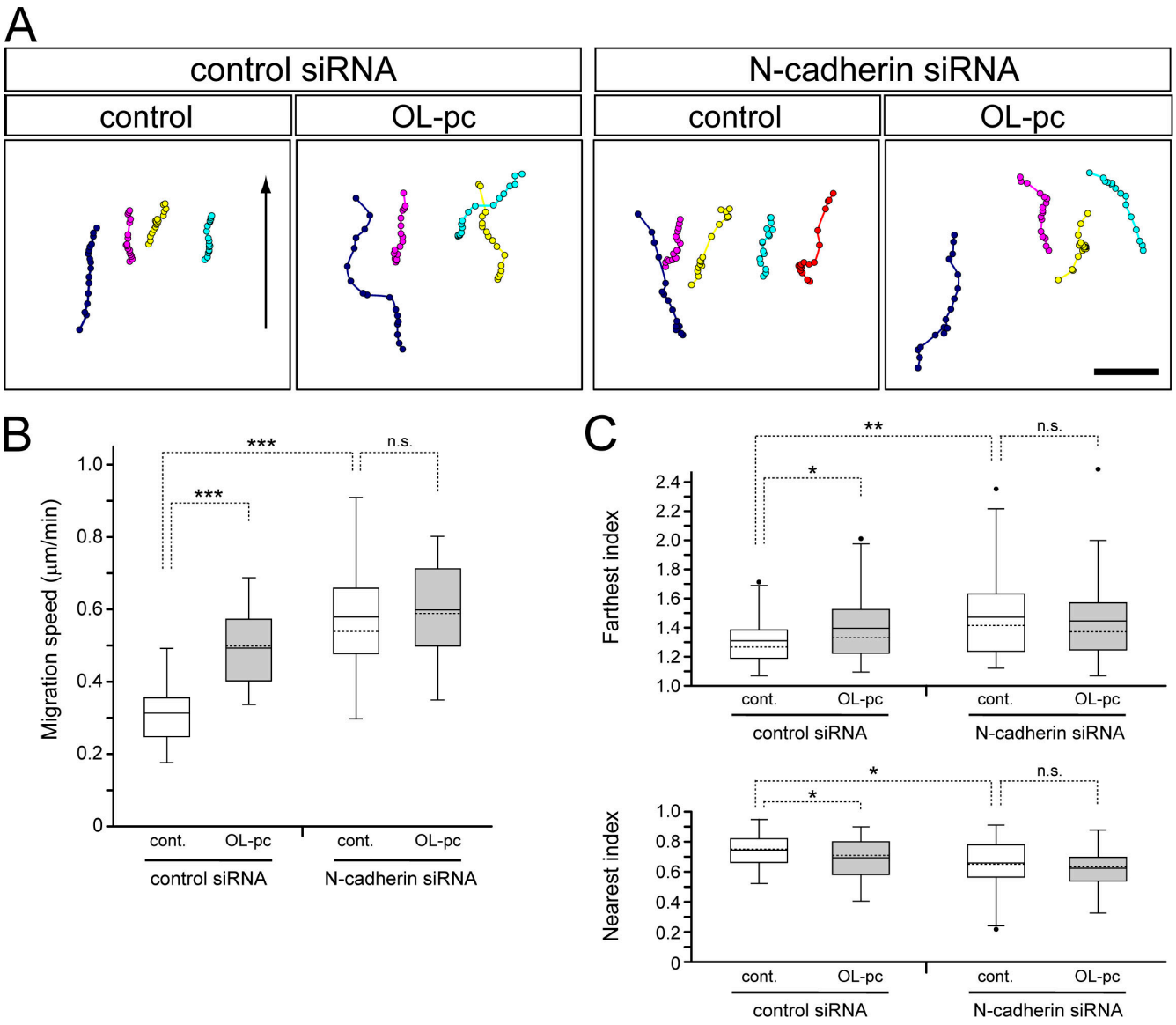

Figure 8. **N-cadherin depletion mimics OL-pc expression.** (A) Control U251 cells and OL-pc-HA transfectants were treated with control or N-cadherin siRNA, and their migration profiles during would healing were analyzed as described in Fig. 5. Time-lapse photographs and videos are available in Fig. S4 and Videos 8 and 9 (available at http://www.jcb.org/cgi/content/full/jcb.200802069/DC1). (B) Quantification of the instantaneous velocities of cells treated with control or N-cadherin siRNA. See Fig. 5 for the method of statistical analysis. *n* = 22 and 20 for control and OL-pc transfectants, respectively, treated with control siRNA; *n* = 19 and 20 for control and OL-pc transfectants, respectively, treated with N-cadherin siRNA. ***, P < 0.0005. n.s., P = 0.68. (C) The farthest and nearest indices obtained as in Fig. 5 D. *n* = 38 and 39 for control and OL-pc transfectants treated with control siRNA, respectively; *n* = 40 and 41 for control and OL-pc transfectants treated with N-cadherin siRNA, respectively. *, P < 0.05; **, P < 0.005. n.s., P = 0.56 and 0.13 for the farthest and nearest indices, respectively. Bar, 50 μm.

Antibodies

mAbs 4F5 and 5E3 against Nap1 were generated by immunizing 7-wk-old Donryu rats (Japan SLC, Inc.) with a keyhole limpet hemocyanin–conjugated mouse Nap1 peptide, CLRNAYHAVYKQSVTSSA, synthesized by Invitrogen. In brief, rats were injected with the synthetic peptides four times at 2-wk intervals, and then the splenocytes of immunized rats were recovered and fused with P3-X63-Ag-U1 myeloma cells (animals were immunized and killed according to the guidelines of the RIKEN Center for Developmental Biology). 4F5 and 5E3 mAbs thus obtained gave a single major band in Western blotting (Fig. S5, available at http://www.jcb.org/cgi/content/full/jcb.200802069/DC1). We mainly used 4F5 for immunohistochemistry and 5E3 for Western blotting. Rat mAb 5G10 against mouse OL-pc was described previously (Aoki et al., 2003). Rabbit pAb against WAVE1 was a gift from T. Takenawa (Kobe University, Kobe, Japan). The following antibodies were purchased: rabbit pAbs against p125Nap1, PIR121-1/Sra-1, and p34-Arc/ARPC2 (Millipore); rabbit pAb against Abi-1 (MBL International); rabbit pAb against N-cadherin (Takara Bio); rat mAb against GFP (Nacalai Tesque); rat anti-HA mAb 3F10 (Roche); mouse anti-HA mAb 16B12 (Covance); rabbit anti-Myc pAb (Santa Cruz Biotechnology, Inc.); and mouse anti-FLAG mAb M2 and anti–α-tubulin mAb DM1A (Sigma-Aldrich). The following were used as secondary antibodies: goat AlexaFluor488, -555, or -647–conjugated anti–mouse IgG or anti–rabbit IgG (Invitrogen); goat Cy3-conjugated anti–rat IgG (Millipore); donkey Cy2-conjugated anti–rat IgG and donkey HRP-conjugated anti–rat IgG (Jackson ImmunoResearch Laboratories); and sheep HRP-conjugated anti–mouse IgG and donkey HRP-conjugated anti–rabbit IgG (GE Healthcare). F-actin was visualized by using AlexaFluor488–conjugated phalloidin (Invitrogen).

RNAi

All siRNAs were purchased (Stealth siRNA; Invitrogen). The target sense sequences that were mainly used are as follows: for human Nap1, 5′-CAACCUUGAUAAGUUGCACACUGCA-3′; for human WAVE1, 5′-AACUGGUACAGUCUCACAUACUGGG-3′; and for human N-cadherin, 5′-AAUUAAGGGAGCUCAAGGACCCAGC-3′. We chose these sequences

from three different sequences for each gene as those that most effectively knocked down the respective gene expression. Negative control stealth siRNAs were also obtained from Invitrogen. As a control for NAP1 RNAi, the scrambled siRNA sequence 5′-CAAGUUAUAUGACGUACAUCCC-GCA-3′ was used. All siRNAs were transfected by use of Lipofectamine RNAiMAX reagent (Invitrogen). The efficiency of gene product suppression was assessed by Western blotting and immunofluorescence staining of cells. In each RNAi-treated culture, >90% of the original protein expression was suppressed by 3–4 d after transfection (Fig. S2).

Live cell imaging and data processing

Time-lapse images were obtained by using a microscope (DeltaVision; Applied Precision) with observation for 4 h at 3-min intervals unless otherwise noted. 2 h before taking videos, the medium was changed to L-15 medium (Invitrogen) supplemented with 10% FCS. For videos of low density cell cultures, 10^4 cells were placed on collagen-coated glass-based dishes (35 mm in diameter; Iwaki) 1 d before the assay. For videos of wound-healing cells, 10^6 cells were placed on noncoated glass-based dishes (35 mm in diameter; Iwaki) and cultured to confluence for 1–2 d. Then, we changed the medium to L-15 medium supplemented with 10% FCS. Wound edges were generated by scraping the cells with a plastic tip, and time-lapse recordings were subsequently started. For tracing fluorescently labeled cells in confluent cultures, we incubated the cells with 30 mM 5(-6) carboxyfluorescein diacetate succinimidyl ester in Hepes-buffered saline for 1 h at room temperature. The labeled cells were then collected by trypsinization and plated together with nonlabeled cells at a 1:10 ratio. After 24–36 h of incubation, the labeled cells were traced at 9-min intervals for another 6 h. In all of these experiments, the dishes were placed on the stage of a microscope (IX71; Olympus) equipped with a cooled CCD camera (Series 300 CH350; Photometrics). The stage was maintained at 37°C by using a thermal controller (Sanyo). Digital images were processed by using SoftWoRx (Applied Precision). For long-term observations of wound healing, images were taken with a system (CV100; Olympus) equipped with a CCD camera in a CO_2 incubator. Trace drawing and statistical analyses were performed with MetaMorph Offline (MDS Analytical Technologies) and Excel (Microsoft), respectively.

Immunofluorescence staining

Cells plated on collagen-coated coverslips (Iwaki) were fixed with 4% PFA in HBSS for 10 min and permeabilized with 0.25% Triton X-100 in TBS for 8 min or 1% Triton X-100 for 10 min. The latter treatment was used for N-cadherin immunostaining. Specimens were incubated with the blocking buffer (5% skim milk in TBS) for 1 h, with the corresponding primary antibodies at several dilutions for 2 h and with the secondary antibodies for 1 h. Coverslips were mounted in FluorSave (EMD) and imaged through plan-Apochromat 63×1.40 NA objectives by use of a fluorescence microscope (Axioplan 2; Carl Zeiss, Inc.) connected with a CCD camera (AxioCam HRc; Carl Zeiss, Inc.) or a laser-scanning confocal microscope (LSM510; Carl Zeiss, Inc.) mounted on an inverted microscope (Axiovert 200M; Carl Zeiss, Inc.), and images were processed using Photoshop (Adobe). For detergent extraction before fixation, cells were treated with a Triton X-100 buffer (50 mM NaCl, 10 mM Pipes, pH 6.8, 3 mM $MgCl_2$, 0.5% Triton X-100, and 300 mM sucrose; Yamazaki et al., 2007) for 10 min on ice and fixed with 4% PFA.

Immunoprecipitation

COS-7 cells transiently cotransfected with FLAG-tagged OL-pc and HA-tagged Nap1 or Myc-tagged CYFIP-2 were harvested and dissolved in the lysis buffer (20 mM Tris-HCl, pH 7.5, 150 mM NaCl, 0.5% Triton X-100, 5% glycerol, 1 mM PMSF, and Complete EDTA-free tablet [Roche]). Lysates were precleared with protein G–Sepharose 4FF beads (GE Healthcare) for 1 h, incubated with antibodies against each tag for 2 h, and incubated with newly prepared protein G–Sepharose 4FF beads for 1 h. The beads were washed three times with the lysis buffer. Precipitates were separated by SDS-PAGE and analyzed by immunoblotting.

Pull-down assay and mass spectrometric analysis

GST fusion proteins containing various deletions of OL-pc cytoplasmic domain (Fig. 1) were expressed in DH5α cells with pGEX-6p-1 vector (GE Healthcare) and were purified. 1-d-old ICR mouse brains were homogenized and lysed in the lysis buffer with 1 mM EDTA and 0.5 mM DTT. Then, the lysate was incubated for 1 h with GST-tagged proteins and glutathione–Sepharose 4B beads (GE Healthcare). The beads were subsequently washed three times in the lysis buffer containing 1 mM EDTA and 0.5 mM DTT. Precipitates were separated by SDS-PAGE and detected by use of 2D Silver Stain (Daiichi), Silver Stain MS kit (Wako), or by Western blot analysis. Each silver-stained precipitate was identified by LC-MS/MS analysis in the Mass Spectrometry Analysis Laboratory in the RIKEN Center for Developmental Biology.

Western blot analysis

Samples were eluted by boiling them in SDS sample buffer (0.25 M Tris-HCl, pH 6.8, 4% SDS, 40% glycerol, and 0.002% bromophenol blue), separated by SDS-PAGE, and transferred to Immobilon-P membranes (Millipore). Membranes were blocked with 5% skim milk in TBS for 1 h and subsequently exposed to primary antibodies for 2 h and then to secondary antibodies for 1 h. The proteins were detected by use of the ECL Plus system (GE Healthcare).

Statistical analysis and data presentation

The box and whisker plots were presented in the following ways (Zisman et al., 2007): the top and bottom ends of the boxes are the 75th and 25th percentiles, respectively. The lines and dashed lines across the box identify the mean and median, respectively. Dots out of the whiskers indicate outliers. The horizontal lines above the boxes represent the maximum datum points or, in the case of the existence of outliers, the outermost datum points that fall within the 75th percentile plus 1.5 times the value of the interquartile range (75th − 25th percentile). The same applies for the lines below the boxes. The data were analyzed by conducting Welch's *t* test.

Online supplemental material

Fig. S1 shows double immunostaining for OL-pc and ARPC2. Fig. S2 shows the knockdown efficiencies of the siRNAs used. Fig. S3 presents still images of cells treated with Nap1 or WAVE1 siRNA. Fig. S4 shows time-lapse images of cells after depletion of Nap1, WAVE1, or N-cadherin. Fig. S5 shows the specificity of anti-Nap1 mAbs. Videos 1–9 show time-lapse images of control (Video 1) and OL-pc transfectants (Video 2) in low density cultures; control (Video 3), OL-pc (Video 4), and OL-pcΔNBS (Video 5) transfectants during wound healing; Nap1-depleted control (Video 6) and OL-pc (Video 7) transfectants during wound healing; and N-cadherin–depleted control (Video 8) and OL-pc (Video 9) transfectants during wound healing. Online supplemental material is available at http://www.jcb.org/cgi/content/full/jcb.200802069/DC1.

We thank D. Yamazaki and T. Takenawa for reagents and helpful discussions; S.T. Suzuki for valuable information; T. Ichii for the homemade programs to analyze live cell imaging; H. Ishigami, M. Nomura, M. Uemura, and C. Yoshii for technical assistance; and Y. Takamiya for the maintenance and preparation of animals.

This work was supported by a grant from the program Grants-in-Aid for Specially Promoted Research of the Ministry of Education, Science, Sports and Culture of Japan to M. Takeichi and by grants-in-aid for scientific research from the Japan Society for the Promotion of Science for Junior Scientists to S. Nakao and for foreign researchers to A. Platek.

Submitted: 19 February 2008
Accepted: 27 June 2008

References

Abe, K., and M. Takeichi. 2008. EPLIN mediates linkage of the cadherin catenin complex to F-actin and stabilizes the circumferential actin belt. *Proc. Natl. Acad. Sci. USA.* 105:13–19.

Abercrombie, M. 1967. Contact inhibition: the phenomenon and its biological implications. *Natl. Cancer Inst. Monogr.* 26:249–277.

Abercrombie, M., and E.J. Ambrose. 1958. Interference microscope studies of cell contacts in tissue culture. *Exp. Cell Res.* 15:332–345.

Aoki, E., R. Kimura, S.T. Suzuki, and S. Hirano. 2003. Distribution of OL-protocadherin protein in correlation with specific neural compartments and local circuits in the postnatal mouse brain. *Neuroscience.* 117:593–614.

Blagg, S.L., and R.H. Insall. 2004. Control of SCAR activity in *Dictyostelium discoideum*. *Biochem. Soc. Trans.* 32:1113–1114.

Bracke, M.E., H. Depypere, C. Labit, V. Van Marck, K. Vennekens, S.J. Vermeulen, I. Maelfait, J. Philippe, R. Serreyn, and M.M. Mareel. 1997. Functional downregulation of the E-cadherin/catenin complex leads to loss of contact inhibition of motility and of mitochondrial activity, but not of growth in confluent epithelial cell cultures. *Eur. J. Cell Biol.* 74:342–349.

Chen, W.C., and B. Obrink. 1991. Cell-cell contacts mediated by E-cadherin (uvomorulin) restrict invasive behavior of L-cells. *J. Cell Biol.* 114:319–327.

Chen, X., and B.M. Gumbiner. 2006. Paraxial protocadherin mediates cell sorting and tissue morphogenesis by regulating C-cadherin adhesion activity. *J. Cell Biol.* 174:301–313.

Fujito, T., W. Ikeda, S. Kakunaga, Y. Minami, M. Kajita, Y. Sakamoto, M. Monden, and Y. Takai. 2005. Inhibition of cell movement and proliferation by cell-cell contact-induced interaction of Necl-5 with nectin-3. *J. Cell Biol.* 171:165–173.

Hirano, S., Q. Yan, and S.T. Suzuki. 1999. Expression of a novel protocadherin, OL-protocadherin, in a subset of functional systems of the developing mouse brain. *J. Neurosci.* 19:995–1005.

Hirano, S., S.T. Suzuki, and C. Redies. 2003. The cadherin superfamily in neural development: diversity, function and interaction with other molecules. *Front. Biosci.* 8:d306–d355.

Hummel, T., K. Leifker, and C. Klämbt. 2000. The *Drosophila* HEM-2/NAP1 homolog KETTE controls axonal pathfinding and cytoskeletal organization. *Genes Dev.* 14:863–873.

Huttenlocher, A., M. Lakonishok, M. Kinder, S. Wu, T. Truong, K.A. Knudsen, and A.F. Horwitz. 1998. Integrin and cadherin synergy regulates contact inhibition of migration and motile activity. *J. Cell Biol.* 141:515–526.

Ibarra, N., A. Pollitt, and R.H. Insall. 2005. Regulation of actin assembly by SCAR/WAVE proteins. *Biochem. Soc. Trans.* 33:1243–1246.

Ibarra, N., S.L. Blagg, F. Vazquez, and R.H. Insall. 2006. Nap1 regulates *Dictyostelium* cell motility and adhesion through SCAR-dependent and -independent pathways. *Curr. Biol.* 16:717–722.

Joslin, E.J., L.K. Opresko, A. Wells, H.S. Wiley, and D.A. Lauffenburger. 2007. EGF-receptor-mediated mammary epithelial cell migration is driven by sustained ERK signaling from autocrine stimulation. *J. Cell Sci.* 120:3688–3699.

Kametani, Y., and M. Takeichi. 2007. Basal-to-apical cadherin flow at cell junctions. *Nat. Cell Biol.* 9:92–98.

Kazmierczak, P., H. Sakaguchi, J. Tokita, E.M. Wilson-Kubalek, R.A. Milligan, U. Muller, and B. Kachar. 2007. Cadherin 23 and protocadherin 15 interact to form tip-link filaments in sensory hair cells. *Nature.* 449:87–91.

Marston, D.J., S. Dickinson, and C.D. Nobes. 2003. Rac-dependent trans-endocytosis of ephrinBs regulates Eph-ephrin contact repulsion. *Nat. Cell Biol.* 5:879–888.

Mege, R.M., J. Gavard, and M. Lambert. 2006. Regulation of cell-cell junctions by the cytoskeleton. *Curr. Opin. Cell Biol.* 18:541–548.

Nakao, S., M. Uemura, E. Aoki, S.T. Suzuki, M. Takeichi, and S. Hirano. 2005. Distribution of OL-protocadherin in axon fibers in the developing chick nervous system. *Brain Res. Mol. Brain Res.* 134:294–308.

Otani, T., T. Ichii, S. Aono, and M. Takeichi. 2006. Cdc42 GEF Tuba regulates the junctional configuration of simple epithelial cells. *J. Cell Biol.* 175:135–146.

Pankov, R., Y. Endo, S. Even-Ram, M. Araki, K. Clark, E. Cukierman, K. Matsumoto, and K.M. Yamada. 2005. A Rac switch regulates random versus directionally persistent cell migration. *J. Cell Biol.* 170:793–802.

Pollard, T.D., and G.G. Borisy. 2003. Cellular motility driven by assembly and disassembly of actin filaments. *Cell.* 112:453–465.

Rakeman, A.S., and K.V. Anderson. 2006. Axis specification and morphogenesis in the mouse embryo require Nap1, a regulator of WAVE-mediated actin branching. *Development.* 133:3075–3083.

Redies, C., K. Vanhalst, and F. Roy. 2005. delta-Protocadherins: unique structures and functions. *Cell. Mol. Life Sci.* 62:2840–2852.

Ridley, A.J., M.A. Schwartz, K. Burridge, R.A. Firtel, M.H. Ginsberg, G. Borisy, J.T. Parsons, and A.R. Horwitz. 2003. Cell migration: integrating signals from front to back. *Science.* 302:1704–1709.

Robinson, R.C., K. Turbedsky, D.A. Kaiser, J.B. Marchand, H.N. Higgs, S. Choe, and T.D. Pollard. 2001. Crystal structure of Arp2/3 complex. *Science.* 294:1679–1684.

Sasaki, N., H. Miki, and T. Takenawa. 2000. Arp2/3 complex-independent actin regulatory function of WAVE. *Biochem. Biophys. Res. Commun.* 272:386–390.

Smith, A., V. Robinson, K. Patel, and D.G. Wilkinson. 1997. The EphA4 and EphB1 receptor tyrosine kinases and ephrin-B2 ligand regulate targeted migration of branchial neural crest cells. *Curr. Biol.* 7:561–570.

Steffen, A., K. Rottner, J. Ehinger, M. Innocenti, G. Scita, J. Wehland, and T.E. Stradal. 2004. Sra-1 and Nap1 link Rac to actin assembly driving lamellipodia formation. *EMBO J.* 23:749–759.

Steffen, A., J. Faix, G.P. Resch, J. Linkner, J. Wehland, J.V. Small, K. Rottner, and T.E. Stradal. 2006. Filopodia formation in the absence of functional WAVE- and Arp2/3-complexes. *Mol. Biol. Cell.* 17:2581–2591.

Stradal, T.E., and G. Scita. 2006. Protein complexes regulating Arp2/3-mediated actin assembly. *Curr. Opin. Cell Biol.* 18:4–10.

Takeichi, M. 1977. Functional correlation between cell adhesive properties and some cell surface proteins. *J. Cell Biol.* 75:464–474.

Takeichi, M. 2007. The cadherin superfamily in neuronal connections and interactions. *Nat. Rev. Neurosci.* 8:11–20.

Takenawa, T., and S. Suetsugu. 2007. The WASP-WAVE protein network: connecting the membrane to the cytoskeleton. *Nat. Rev. Mol. Cell Biol.* 8:37–48.

Uemura, M., S. Nakao, S.T. Suzuki, M. Takeichi, and S. Hirano. 2007. OL-protocadherin is essential for growth of striatal axons and thalamocortical projections. *Nat. Neurosci.* 10:1151–1159.

Vaezi, A., C. Bauer, V. Vasioukhin, and E. Fuchs. 2002. Actin cable dynamics and Rho/Rock orchestrate a polarized cytoskeletal architecture in the early steps of assembling a stratified epithelium. *Dev. Cell.* 3:367–381.

Vaheri, A., E. Ruoslahti, B. Westermark, and J. Ponten. 1976. A common cell-type specific surface antigen in cultured human glial cells and fibroblasts: loss in malignant cells. *J. Exp. Med.* 143:64–72.

Vanhalst, K., P. Kools, K. Staes, F. van Roy, and C. Redies. 2005. delta-Protocadherins: a gene family expressed differentially in the mouse brain. *Cell. Mol. Life Sci.* 62:1247–1259.

Watanabe, T., J. Noritake, and K. Kaibuchi. 2005. Regulation of microtubules in cell migration. *Trends Cell Biol.* 15:76–83.

Yamazaki, D., T. Oikawa, and T. Takenawa. 2007. Rac-WAVE-mediated actin reorganization is required for organization and maintenance of cell-cell adhesion. *J. Cell Sci.* 120:86–100.

Yasuda, S., H. Tanaka, H. Sugiura, K. Okamura, T. Sakaguchi, U. Tran, T. Takemiya, A. Mizoguchi, Y. Yagita, T. Sakurai, et al. 2007. Activity-induced protocadherin arcadlin regulates dendritic spine number by triggering N-cadherin endocytosis via TAO2beta and p38 MAP kinases. *Neuron.* 56:456–471.

Yokota, Y., C. Ring, R. Cheung, L. Pevny, and E.S. Anton. 2007. Nap1-regulated neuronal cytoskeletal dynamics is essential for the final differentiation of neurons in cerebral cortex. *Neuron.* 54:429–445.

Zisman, S., K. Marom, O. Avraham, L. Rinsky-Halivni, U. Gai, G. Kligun, V. Tzarfaty-Majar, T. Suzuki, and A. Klar. 2007. Proteolysis and membrane capture of F-spondin generates combinatorial guidance cues from a single molecule. *J. Cell Biol.* 178: 1237–1249.